Switching dynamics and surface forces in thresholdless "V-shaped" switching ferroelectric liquid crystals

Michael J. O'Callaghan*
Displaytech, Inc., 2602 Clover Basin Drive, Longmont, Colorado 80503
(Received 23 August 2002; published 31 January 2003)

The electrostatic model of thresholdless V-shaped switching is able to explain the general low frequency (quasistatic) electro-optic behavior of smectic-C^* ferroelectric liquid crystals (vFLCs). Here, dynamical equations based on the electrostatic model are developed which predict a vFLC cell's small-amplitude switching speed and which also show that a strongly amplitude-dependent switching speed is expected. A relationship between the switching time constants of analog vFLCs and of the faster, yet structurally similar, binary FLCs is found. The electrostatic model applies in the limit where the FLC's spontaneous polarization is large enough to completely overwhelm surface and elastic forces. This analysis suggests that, in many cases of practical interest, electrostatic energies may be low enough for surface forces to play an important role even when the director structure is strongly stiffened by a large polarization charge. It is shown that the addition of surface forces to the electrostatic model can improve agreement between the model and the observed dynamical response of vFLC cells.

DOI: 10.1103/PhysRevE.67.011710 PACS number(s): 61.30.Cz, 61.30.Gd, 42.79.Kr

I. INTRODUCTION

Since the initial observation of thresholdless (V-shaped) switching [1], an electrostatic model of ferroelectric smectic-C^* liquid crystals (vFLCs) has been developed to explain its general analog electro-optic characteristics [2,3]. The model predicts that under certain conditions (e.g., large spontaneous polarization), the FLC's director structure becomes spatially uniform (''stiffened'') and that surface anchoring energies become overwhelmed and can be neglected. Under these conditions, the steady-state voltage dependence of a vFLC's optic axis position is determined by just three parameters: the vFLC's spontaneous polarization P_S, the alignment layer's thickness t_A and dielectric constant ε_A.

vFLC cells are often studied using low frequency drive wave forms so that the vFLC is in near-static equilibrium with the applied voltage (where the steady-state electrostatic model applies), i.e., $1/f \gg \tau$, where τ, is the characteristic response time of the cell and f is the drive frequency. At even lower frequencies, the idealized ''V'' distorts to become a ''W'' due to ionic charge flow [4,5] (optic axis motion leads the drive waveform). At higher drive frequencies, where $1/f$ is comparable to or less than τ, optic axis motion substantially lags the drive wave form. Neither the high frequency behavior nor the value of τ are accounted for by the quasistatic electrostatic model. The apparent slow speed of vFLCs has also been puzzling. FLCs are known for their high switching speeds when operated as binary electro-optic modulators [6] yet vFLCs, thought to have essentially the same structure, seem much slower.

Here, the electrostatic model is analyzed to understand its switching dynamics and to quantitatively assess the importance of surface forces. We find that in many FLC cells of practical interest, we should expect the bulk of the FLC to be stiffened, yet the strength of the electrostatic effect is not so large that surfaces can be neglected. To account for this, simple models for surface anchoring forces have been added to the electrostatic model. The resulting dynamical equation has been used to numerically simulate vFLC switching and the result is compared to the dynamic response of a high-P_S smectic-C^* FLC cell. The computed vFLC switching time constant was found to be close to the measured value.

II. THE ELECTROSTATIC MODEL

Figure 1 is an illustration of the surface stabilized smectic-C^* bookshelf structure (suppressed helix), in which the FLC molecules organize themselves into sheets (smectic layers). The FLC molecules' electric dipoles are confined to rotate within the smectic planes, while the molecule's long axes ($\sim$ the director) are constrained to tilt away from the layer normal by a fixed angle θ. This is also the direction of the optical index ellipsoid's extraordinary axis. As the director rotates through the angle ϕ around the layer normal

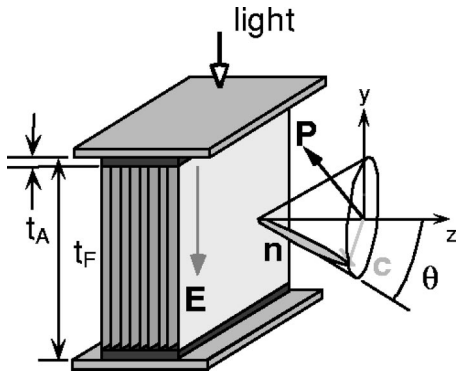

FIG. 1. Illustration showing bookshelf vFLC smectic layers, the orientation of the FLC dipoles **P**, and the director/index ellipsoid axis c.

*Electronic address: mikeo@displaytech.com

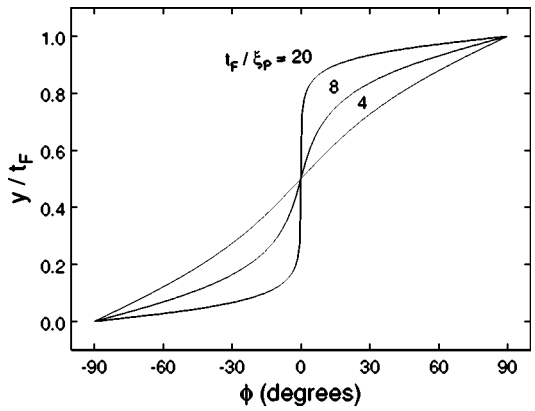

FIG. 2. Computed curves of dipole orientation ϕ vs position between cell faces for three ratios of FLC thickness t_F to characteristic length ξ_P.

(driven by an applied electric field $\boldsymbol{E}$), the projection of the index ellipsoid onto the cell face changes, causing the cell's optic axis to rotate. In general, ϕ will vary throughout the volume of a cell in response to surface forces, bulk elastic properties, and electrostatics. In the model for vFLC cells, however, the FLC spontaneous polarization P_S is large and electrostatic forces drive the FLC dipoles to everywhere point in the same direction.

In a cell whose surfaces favor polar anchoring the dipoles will tend to point into (or out of) the cell's top and bottom surfaces. If P_S is small then the dipole will rotate linearly from one surface to the other as indicated by the curve labeled ''4'' in Fig. 2. As P_S is increased, electrostatic forces will drive the dipoles in the bulk to align with an angle of $\phi=0$ (i.e., so that they are parallel to the cell faces). Larger values of P_S cause the regions in which ϕ varies to match the surfaces (twist regions) to become progressively thinner.

The characteristic length that sets the approximate thickness of the twist regions [6,7] is

$$\xi_P=\sqrt{\varepsilon_F B}/P_S, \tag{1}$$

where B is an elastic constant of the FLC and ε_F is its dielectric constant. The FLC structure becomes ''stiffened'' once ξ_P becomes much less than the cell thickness t_F (i.e., $\xi_P/t_F \ll 1$). The force with which the bulk pulls on the surface grows as ξ_P shrinks, eventually reaching a point where surface forces are overwhelmed. In this extreme case, dipoles throughout the FLC (even at the surface) all point in the same direction and it has been assumed that surface interactions can be ignored in this limit.

Once director stiffening has been achieved and surface interactions become negligible, calculation of the FLC's response to an applied voltage becomes very simple as illustrated in Fig. 3. In the vFLC electrostatic model, the FLC dipoles rotate to screen the applied electric field and the field inside the FLC is always zero (if the applied voltage does not exceed a saturation value V_S). If the electric field generated by electrical charge on the cell's electrodes is E then the voltage across the cell must be $V=2Et_A/(\varepsilon_A/\varepsilon_0)$, where t_A is the alignment layer's thickness and ε_A is its dielectric

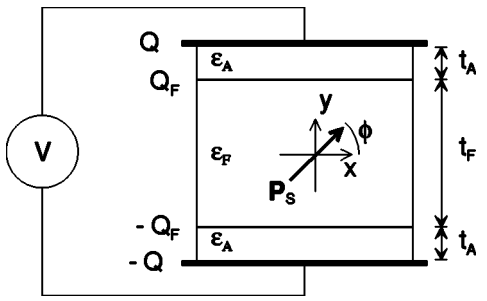

FIG. 3. Illustration of the electronic equivalent circuit.

constant. Charge density on the FLC layer's surface due to its spontaneous polarization P_S is equal to $P_S\sin\phi$ and the electric field within the FLC layer is $\varepsilon_0 E/\varepsilon_F + P_S\sin\phi/\varepsilon_F$ where ε_F is the FLC's dielectric constant. The applied electric field is screened when the dipole orientation ϕ satisfies the condition $\varepsilon_0 E=-P_S\sin\phi$, or equivalently when $V=-2t_A P_S\sin\phi/\varepsilon_A$. Maximum rotation of the dipole from its equilibrium position at $\phi=0$ occurs for $V=\pm V_S$ where $V_S=2t_A P_S/\varepsilon_A$.

III. DYNAMICS OF THE ELECTROSTATIC MODEL

Inspection of Fig. 3 shows that $V=-2E_A t_A - E_F t_F$, where E_A and E_F are the electric fields within the alignment layers and FLC layer, respectively. The electrical charge on the surface of the FLC layer is related to the electric fields by $Q_F/A=\varepsilon_A E_A-\varepsilon_F E_F$, where A is the cell's surface area. The charge Q_F is related to the FLC dipole orientation through $Q_F/A=P_S\sin\phi$, where P_S is the magnitude of the FLC's spontaneous polarization. These relationships are combined to determine the electric field within the FLC layer:

$$E_F=-\frac{V+V_S\sin\phi}{t_F+2t_A\dfrac{\varepsilon_F}{\varepsilon_A}}, \quad V_s=\frac{2t_A P_s}{\varepsilon_A}. \tag{2}$$

The electric field E_F applies a torque to the FLC which drives its motion. Making the usual assumption of viscosity-limited dynamics (i.e., no momentum terms), the equation governing director dynamics becomes

$$\frac{d\phi}{dt}=\frac{1}{\eta}E_F P_S\cos\phi \Rightarrow \frac{d\phi}{dt}=-\frac{1}{\tau_0}\left(\frac{V}{V_S}+\sin\phi\right)\cos\phi, \tag{3}$$

$$\tau_0=\frac{\eta}{P_S^2}\left(\varepsilon_F+\frac{t_F}{2t_A}\varepsilon_A\right).$$

The effects of dielectric anisotropy have been omitted. Appendix A shows that, in cases of interest here, the dielectric anisotropy has only a small effect and can be neglected.

Torque applied by the electric field is largest near $\phi=0$ and drops to zero at $\phi=\pm\pi/2$ (where the electric field is parallel to the dipole). This suggests that the FLC's response time τ should be smallest near $\phi=0$ and should increase as

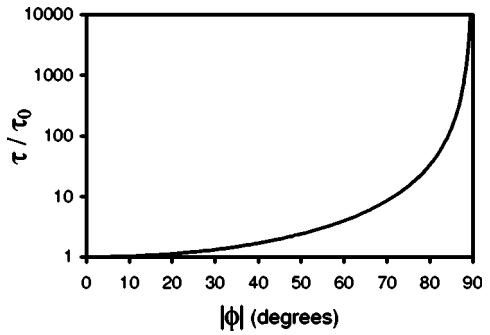

FIG. 4. The characteristic response time of the vFLC increases as the FLC dipoles become more parallel to the electric field ($|\phi| = 90°$).

ϕ approaches $\pm\pi/2$. We can determine a ϕ-dependent time constant from the above equation by linearizing it in the case of an applied voltage $V(t)=V+v(t)$, where V is a constant and $v(t)$ is small. The time-dependent voltage $v(t)$ drives small variations of ϕ about the position ϕ_V:

$$\frac{d\tilde{\phi}}{dt} = -\frac{1}{\tau_0}\frac{v}{V_S} - \frac{1}{\tau}\tilde{\phi}, \tag{4}$$

$$\tilde{\phi} = \phi - \phi_V, \quad \sin\phi_V = -\frac{V}{V_S}, \quad \tau = \frac{\tau_0}{\cos^2\phi_V}.$$

Here, τ is the time constant for small motions of the dipole near the equilibrium position ϕ_V and τ_0 is the value of the time constant at $V=0$ (where $\phi=0$). The ratio τ/τ_0 vs ϕ is plotted in Fig. 4. As expected, it grows to infinity as ϕ approaches 90°.

Figure 5 shows numerical simulations of dipole orientation ϕ vs time for small-amplitude square wave drive ($|V/V_S|=0.01$ at 50 Hz) and for large-amplitude drive ($|V/V_S|=1$ at 5 Hz). The vFLC time constant was set to

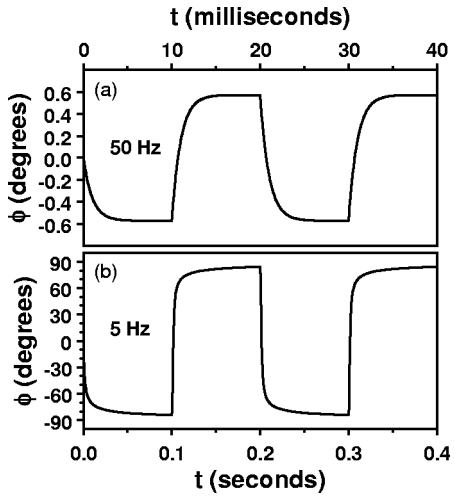

FIG. 5. (a) Numerical simulation of $\phi(t)$ for a vFLC with $\tau_0 = 1$ ms driven by a 50 Hz square wave with $|V/V_S|=0.01$. (b) Numerical simulation when driven by a 5-Hz square wave with $|V/V_S|=1$.

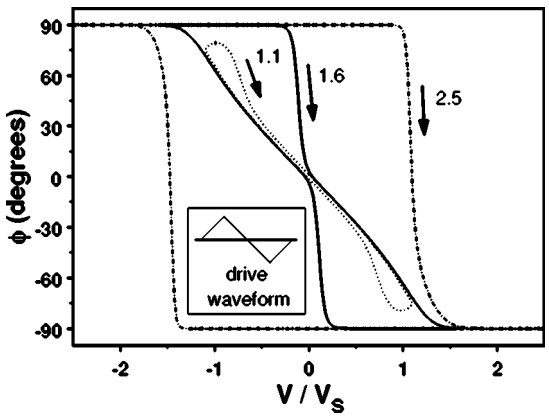

FIG. 6. Computed closed curves of dipole orientation ϕ vs voltage when driven by a 5-Hz triangle wave with amplitude $\pm V_{max}$ (inset). The vFLC time constant is $\tau_0=1$ ms. Curves are shown for $V_{max}/V_S=1.1$, $V_{max}/V_S=1.6$, and $V_{max}/V_S=2.5$. Arrows indicate the trajectory of $\phi(t)$ along the curves for increasing t.

$\tau_0=1$ ms. In the small-amplitude case, the dipole follows the applied voltage with a 1 ms time constant and closely approaches steady-state values of $\pm 0.57°$ within a few milliseconds. In the large-amplitude case, the dipole orientation falls short of its $\phi=\pm 90°$ steady-state values even after 100 ms have elapsed (the half period of the 5-Hz square wave). This is expected from the expression for τ [Eq. (4)], which shows that the time constant diverges to infinity as the dipole approaches $\pm 90°$.

Figure 6 shows curves of ϕ vs V/V_S computed by numerical solution of the time-dependent differential equation [Eq. (3)] with $\tau_0=1$ ms. The vFLC cell is driven by a 5-Hz triangle wave of amplitude $\pm V_{max}$. Curves are shown for three values of V_{max}/V_S. At $V_{max}/V_S=1.1$, the dipoles follow the applied voltage fairly accurately up to about $\phi = \pm 30°$. At the ends of the curve, the time constant has increased by a factor of 10 or more, preventing the dipoles from rotating all the way to $\pm 90°$ in the time allowed by the 5 Hz drive frequency. This leads to formation of the loops seen at the ends of the curve. The larger torque produced in the $V_{max}/V_S=1.6$ case forces the dipoles nearer to $\pm 90°$ where the time constant becomes even larger. The dipoles remain "stuck" near $\pm 90°$ until V/V_S drops to near zero, after which the curve of $\phi(V)$ is very similar to the $V_{max}/V_S=1.1$ case until ϕ again approaches $\pm 90°$. In the case of $V_{max}/V_S=2.5$, the vFLC response effectively becomes that of a binary FLC. Note that this range of behavior occurs at a drive frequency whose period is 200 times the value of the vFLC time constant τ_0.

How does the speed of an analog vFLC cell compare to the speed of an FLC cell operated as a binary optical modulator? In the binary FLC model, the applied voltage drives the dipole to point along the electric field; the dipole is driven either "up" or "down" ($\phi=\pm 90°$) depending on the polarity of the voltage. For the representative set of FLC parameters $t_A=20$ nm, $P_S=30$ nC/cm^2, and $\varepsilon_A=3.5\varepsilon_0$, we find $V_S\cong 0.4$ V, whereas typical drive voltages are 5–10 times larger. The electric field within the FLC layer does not change greatly as the FLC dipoles rotate because the

electric field they produce only partially screens the applied field. The FLC can be driven arbitrarily fast by increasing the drive voltage (ignoring other problems that occur at high voltages in real cells). In contrast, the drive voltage V must always be less than V_S (so that $|\phi|<90°$) in order to obtain analog modulation in vFLCs.

The switching time constant τ_B of a binary FLC cell is given [6] by

$$\tau_B=\frac{\eta}{P_S E}. \tag{5}$$

It is assumed that the electric field driving the dipoles remains constant and is independent of dipole orientation ϕ (equivalent to requiring $V\gg V_S$).

Using Eq. (2) to determine the electric field in the case of $V_S/V\ll 1$, we find a relationship between the FLC time constant and the vFLC time constant.

$$\tau_B=\frac{V_S}{V}\tau_0. \tag{6}$$

This comparison indicates that for a specific set of FLC cell parameters (P_S, t_A, etc.), the time constant for binary FLC switching ($V\gg V_S$) will be less than the small-amplitude vFLC time constant τ_0 by a factor of V_S/V. Binary FLC cells are faster than vFLCs simply because they are driven by larger voltages (compared to V_S), voltages beyond those at which analog behavior is obtained.

IV. INCLUSION OF SURFACE FORCES

The vFLC model assumes that surface interaction forces can be neglected when P_S is sufficiently large, and that the voltage dependent dipole orientation ϕ is constant throughout the vFLC's volume. Observation of vFLC dynamical behavior (Sec. VI), and a review of the energies involved (this section), suggest nevertheless that surface forces may be important in many cases of practical interest.

The total surface free energy (or FLC-to-alignment layer adhesion energy) can be written as

$$\mathcal{F}=\mathcal{F}_I+\mathcal{F}_A, \tag{7}$$

where $\mathcal{F}_I$ is the isotropic part and $\mathcal{F}_A$ is the anisotropic part. Typical values for $\mathcal{F}_I$ when the alignment layer is an organic material are likely on the order of 50 erg/cm^2 [8]. The orientation dependent liquid crystal anchoring energies of interest here are contained in $\mathcal{F}_A$. Nematic liquid crystal anchoring energies [9,10] span the range of 10^{-5}–1 erg/cm^2, with typical values being in the range of 10^{-3}–10^{-2} erg/cm^2. FLC anchoring energies are less well known, typical values may be on the order of 1 erg/cm^2 [11].

This section begins by evaluating the bulk electrostatic energy of a vFLC cell. The relative importance of surface anchoring energy is assessed by comparison with the calculated electrostatic energy. Simple models for surface anchoring are added to the electrostatic model and their effects on switching are evaluated. Two representative cases are considered. First is the case of pinned polar anchoring, in which ϕ is fixed at the surfaces (e.g., Fig. 2). The angle ϕ takes on a different value throughout the bulk and varies linearly near the surfaces to match boundary conditions. This approximates the case of stiffened FLC director structures subject to strong anchoring that have been investigated previously through numerical calculations [6,12,13]. The second case considered here is the one where ϕ is constant all the way to the surface. In this case, the FLC director structure is rigid enough such that surface forces are unable to significantly deform it, yet they remain strong enough to affect switching. Both polar and nonpolar surface forces are considered.

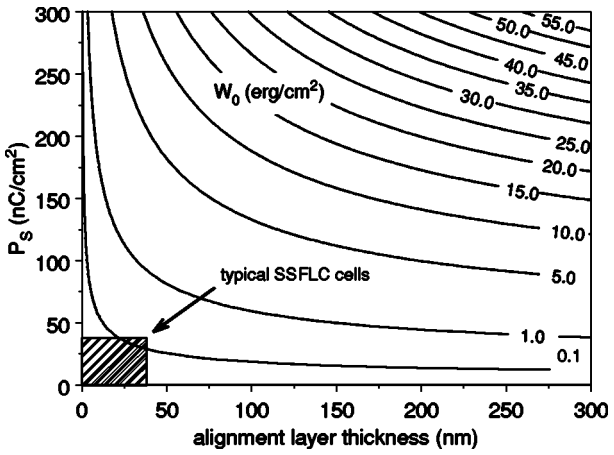

FIG. 7. Contour plot showing electrostatic holding energy W_0 (erg/cm^2) as a function of FLC polarization P_S and alignment layer thickness t_A for an FLC layer thickness of 2 μm. Other assumed values are $\varepsilon_A=3.5\varepsilon_0$, $\varepsilon_F=5\varepsilon_0$.

A. Electrostatic potential energy

Electrostatic forces holding FLC dipoles at their equilibrium position can be characterized by a potential energy function dependent on V and ϕ. The electrostatic potential energy per unit volume is found by integrating the electrostatic torque applied to the dipoles:

$$U(\phi)=-\int_0^{\phi} T(\phi')\,d\phi'=-\int_0^{\phi} E_F P_S\cos\phi'\,d\phi'. \tag{8}$$

Here, E_F is the electric field within the FLC layer [Eq. (2)]. The energy per unit area $W(\phi)$ is obtained by multiplying $U(\phi)$ by the FLC layer thickness:

$$W(\phi)=U(\phi)t_F=W_0\left(\sin^2\phi+2\frac{V}{V_S}\sin\phi\right), \tag{9}$$

$$W_0=\frac{t_A P_s^2}{\varepsilon_A\left(1+\dfrac{\varepsilon_F}{\varepsilon_A}\dfrac{2t_A}{t_F}\right)}, \quad V_S=\frac{2t_A P_S}{\varepsilon_A}.$$

Energy density W_0 scales the depth of the dipole's potential energy well. Figure 7 shows plots of W_0 for a range of spontaneous polarization P_S and alignment layer thickness t_A. Typical FLC cells have P_S values of less than about 30 nC/cm^2 with alignment layer thicknesses of around 30

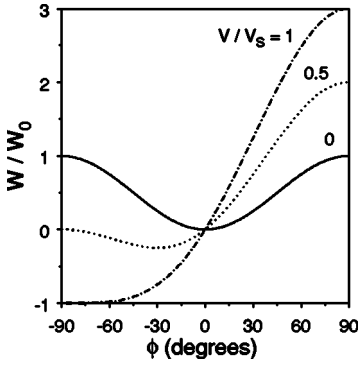

FIG. 8. Curves of normalized electrostatic potential energy W/W_0 vs dipole orientation ϕ.

nm or less. Figure 7 shows that W_0 for such cells is comparable to the upper range of reported surface anchoring energies (10^{-2}–1 erg/cm^2). This suggests that surface anchoring energies are likely to be negligible in comparison to bulk electrostatics only in cells with very high-P_S values and thick alignment layers.

As the alignment layer is made thicker, W_0 saturates at

$$W_0=\frac{t_F P_S^2}{2\varepsilon_F}. \tag{10}$$

For a 2-μm-thick FLC layer with $\varepsilon_A=3.5\varepsilon_0$ and $\varepsilon_F=5\varepsilon_0$, W_0 reaches 90% of its saturation value with a 7-μm alignment layer. With $P_S=100$ nC/cm^2 the saturation value is $W_0\sim 22$ erg/cm^2.

Figure 8 shows plots of $W(\phi)$ for three values of V/V_S. The minima of these potential energy curves are broad rather than sharp, and the minima become flatter and broader as V/V_S increases. The time constant of the vFLC near equilibrium is determined by the first derivative of W so the variation of the minimum's flatness with V/V_S is consistent with the previous calculation of τ [Eq. (4)].

Note that the curve of $W(\phi)$ rises by only $10^{-2}W_0$ between $\phi=90°$ and $\phi=65°$ for $V/V_S=1$. This shows that even though W_0 may be much larger than the surface anchoring energy, the surfaces may still play a significant role in vFLC cells. Since typical values of W_0 are on the order of 10^{-1} erg/cm^2, this suggests that surface anchoring energies as small as 10^{-3} erg/cm^2 may be strong enough to significantly change the equilibrium value of ϕ. Even with large values of W_0, of the order of 10 erg/cm^2 (e.g., $P_S\sim 150$ nC/cm^2, $t_A\sim 200$ nm), reported FLC anchoring energies of 1 erg/cm^2 amount to about $10^{-1}W_0$. So even in the case of moderately large W_0, we find that surface forces are likely to be important.

B. Surface interaction models

The electrostatic model assumes a limit in which $\mathcal{F}_A$ is negligibly small (large P_S). The preceding analysis leads us to expect, however, that $\mathcal{F}_A$ may play an important role in vFLC switching dynamics in cases of practical interest. We anticipate that there will be FLCs whose P_S is large enough for their structure and behavior to approximate that of a vFLC, yet their P_S is not large enough to totally overwhelm surface effects. Here, we consider what the form of $\mathcal{F}_A(\phi)$ might be in these intermediate situations. Two cases are considered. In the first case, we assume that surface anchoring is strong and that the director orientations ϕ_0 and ϕ_L at the surfaces are fixed. In the second case, we assume that the FLC is fully stiffened and that ϕ is everywhere the same.

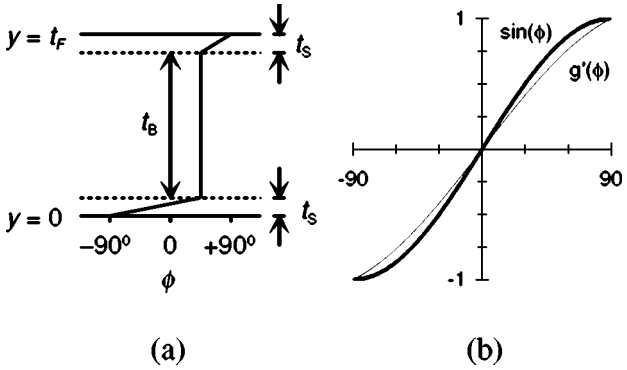

FIG. 9. (a) Illustration of the simplified model for a polarization stiffened FLC with pinned surfaces. The director orientation takes on a constant value within the bulk (thickness t_B) and varies linearly in near-surface layers of thickness t_S to join with the surfaces. (b) Comparison of $g'(\phi)=\varepsilon_F g(\phi)/t_S P_S$ and $\sin\phi$.

1. Pinned surfaces

The model here is the same as for the simpler case of Sec. III except that the FLC layer has been divided into three regions as shown in Fig. 9. In the central region of the FLC layer, ϕ is a constant as before. In the two near-surface regions of FLC (each of thickness t_S), we make the approximation that ϕ varies linearly to join the central bulk value (thickness t_B) with the pinned values at the alignment layer surfaces.

Charge density within the cell is

$$\rho(\mathbf{r})=q(\mathbf{r})-\nabla\cdot\mathbf{P}(\mathbf{r}). \tag{11}$$

We apply Gauss's law making use of the fact that the electric field outside the cell is zero. The integral is evaluated over a volume confined between two infinite planar surfaces, one lying outside the cell and parallel to the cell faces and a second parallel surface within the cell. The electric field at the plane located at y is found to be

$$E(y)=\frac{\varepsilon_A}{\varepsilon(y)}E_A-\frac{1}{\varepsilon(y)}P_y(y),\quad E_A=-\frac{1}{\varepsilon_A}\frac{Q}{A}, \tag{12}$$

where Q is the charge on one of the cell's electrodes as before and $P_y=P_S\sin\phi$ is the y component of polarization vector $\mathbf{P}$. The voltage across the cell is the integral of $-E(y)dy$:

$$V=-E_A\left(\frac{\varepsilon_A}{\varepsilon_F}t_B+\frac{\varepsilon_A}{\varepsilon_F}2t_S+2t_A\right)+\frac{t_B P_S}{\varepsilon_F}\sin\phi+g(\phi), \tag{13}$$

$$g(\phi)=\frac{1}{\varepsilon_F}\int_0^{t_S}P_y(y)dy+\frac{1}{\varepsilon_F}\int_{t_F-t_S}^{t_F}P_y(y)dy$$
$$=-\frac{t_S P_S}{\varepsilon_F}\left[\frac{\cos\phi_{t_F}-\cos\phi}{\phi_{t_F}-\phi}+\frac{\cos\phi-\cos\phi_0}{\phi-\phi_0}\right].$$

Combining Eqs. (12) and (13), we find an expression for the electric field within the FLC,

$$E_F(y)=-\frac{V+V_S\left(1+\frac{\varepsilon_A}{\varepsilon_F}\frac{t_S}{t_A}\right)\sin\phi(y)-g[\phi(y)]}{t_B+2t_S+\frac{\varepsilon_F}{\varepsilon_A}2t_A}. \tag{14}$$

As before, the electrostatic torque acting on the FLC dipoles is integrated to determine the corresponding potential energy function [Eq. (8)]. However, the function $g(\phi)$ complicates evaluation of the integral. Two simplifications are introduced to help with this. First, we set $\phi_0=-\phi_{t_F}=-\pi/2$, consistent with our assumption of pinned polar anchoring. Second, $g(\phi)$ is very similar to the sine function on the interval $-\pi/2\leqslant\phi\leqslant\pi/2$ as shown in Fig. 9, so we make the approximation $g(\phi)\cong t_S P_S\sin\phi/\varepsilon_F$. With this substitution, the integral is readily evaluated and the energy per unit area is found:

$$W(\phi)=U(\phi)t_B=W_0'\left(\sin^2\phi+\frac{V}{V_S'}\sin\phi\right), \tag{15}$$

$$W_0'=W_0\frac{\left(1+\frac{\varepsilon_F}{\varepsilon_A}\frac{2t_A}{t_F}\right)\left(1+\frac{\varepsilon_A}{\varepsilon_F}\frac{t_S}{2t_A}\right)}{\left(1+\frac{\varepsilon_F}{\varepsilon_A}\frac{2t_A}{t_B}+\frac{2t_S}{t_B}\right)}\cong W_0\left(1+\frac{\varepsilon_A}{\varepsilon_F}\frac{t_S}{2t_A}\right),$$

$$V_S'=V_S\left(1+\frac{\varepsilon_A}{\varepsilon_F}\frac{t_S}{2t_A}\right).$$

The above approximation for W_0' applies when $2t_S/t_B\ll 1$, this inequality is satisfied in the stiffened director structure limit studied here.

Now consider the twist regions, in which the energy density is the sum of elastic and electrostatic contributions. We assume the condition $t_S/t_B\ll 1$, so that the electrostatic energy of the twist regions is negligibly small compared to W_0'. A straight line is used in the twist regions to approximate the curve $\phi(y)$ that joins the surface to the bulk (Figs. 2 and 9), the thickness of each twist region is $t_S\cong 2\xi_P$. The elastic energy density is

$$u=\frac{1}{2}B\left(\frac{\partial\phi}{\partial y}\right)^2=\frac{B}{8\xi_P^2}(\phi-\phi_S)^2, \tag{16}$$

where ϕ_S is the dipole orientation at a surface. The elastic energy per unit area of a twist region is

$$W_S(\phi)=\frac{U}{A}=\frac{2\xi_P Au}{A}=\frac{\gamma}{\pi^2}(\phi-\phi_S)^2, \tag{17}$$

$$\gamma\equiv\frac{B\pi^2}{4\xi_P}=\frac{\pi^2}{4}P_S\sqrt{\frac{B}{\varepsilon_F}}.$$

The factor γ scales the surface energy and is defined to be equal to $W_S(\phi)$ at $|\phi-\phi_S|=\pi$. The combined energy of both twist regions (assuming pinned polar anchoring with $\phi_S=\pm\pi/2$) is now

$$W_S(\phi)=\frac{\gamma}{\pi^2}(\phi-\phi_S)^2+\frac{\gamma}{\pi^2}(\phi+\phi_S)^2=\frac{2\gamma}{\pi^2}\phi^2, \tag{18}$$

where the fixed term $(2\gamma/\pi^2)\phi_S^2$ has been omitted because it has no effect on switching behavior.

For representative values of $B=10^{-11}$ N, $P_S=100$ nC/cm^2, and $\varepsilon_F=5\varepsilon_0$, we compute $\gamma=1.3$ erg/cm^2. Measured values of polar anchoring energy for FLCs are also ~ 1 erg/cm^2 [12]. This implies that for such a large surface anchoring energy to be overwhelmed by the elastic energy (i.e., to "break" with the surface) we need $\gamma\gg 1$ erg/cm^2 which in turn implies that we would need $P_S\gg 100$ nC/cm^2.

The ratio of elastic energy to bulk electrostatic energy is

$$\frac{2\gamma}{W_0'}=\frac{\pi^2}{2}\frac{\varepsilon_A}{\varepsilon_F}\frac{\xi_P}{t_A}\frac{\left(1+\frac{\varepsilon_F}{\varepsilon_A}\frac{2t_A}{t_B}+\frac{4\xi_P}{t_B}\right)}{\left(1+\frac{\varepsilon_A}{\varepsilon_F}\frac{\xi_P}{t_A}\right)}, \tag{19}$$

where we have used the approximation $t_S\cong 2\xi_P$. For $\xi_P\sim t_A$ the bulk electrostatic energy and the elastic energy of the thin twist regions are comparable. Therefore, if the surfaces are pinned we can expect the elastic energy to play an important role in switching dynamics unless $\xi_P\ll t_A$.

2. Planar and polar anchoring

In this case, we assume that the vFLC director structure is fully stiffened. The dipole orientation ϕ takes on a single value throughout the FLC layer, even at the surfaces. Although the FLC is fully stiffened in this case, the ϕ-dependent surface interaction energy is still present and will affect the cell's static and dynamic response to applied voltages. Perhaps the most common and simplest approximation of ϕ-dependent surface energy represents it as the sum of a polar contribution γ_P and a nonpolar contribution γ_N [10,14]:

$$\text{at } y=0: W_S(\phi)=+\gamma_P\sin\phi-\gamma_N\sin^2\phi, \tag{20}$$

$$\text{at } y=t_F: W_S(\phi)=-\gamma_P\sin\phi-\gamma_N\sin^2\phi.$$

First, consider the purely polar anchoring case ($\gamma_N=0$). Suppose, for example, that both surfaces prefer the FLC dipole to be pointing into the surface. In this case, the upper

surface contributes an energy of $-\gamma_P \sin\phi$ and the bottom surface contributes $+\gamma_P \sin\phi$. These contributions add to zero.

In the above polar anchoring case $W_S(\phi)$ has a minimum at the $y=0$ surface for $\phi=-90°$. Suppose, instead, that the alignment layer induces a pretilt angle of α, a common situation. The value of ϕ that minimizes $W_S(\phi)$ then satisfies the condition

$$\cos^2\alpha = \cos^2\theta + \sin^2\theta \sin^2\phi, \tag{21}$$

where θ is the FLC's tilt angle. For representative values of $\alpha=5°$ and $\theta=30°$, we find equilibrium values of ϕ at the surfaces to be $\pm 80°$. We can approximate the anisotropic surface energies of the top and bottom surfaces to be, respectively, $-\gamma_P \sin(\phi+\Delta)$ and $+\gamma_p \sin(\phi-\Delta)$ where in the above example, we would set $\Delta=10°$. Summing these together we find that the total anisotropic surface energy no longer adds to zero.

$$W_S(\phi) = -2\gamma_P \sin\Delta \cos\phi. \tag{22}$$

In the case of purely nonpolar anchoring ($\gamma_P=0$), the energies of the two surfaces add to become $-2\gamma_N \sin^2\phi$. A potential of this form has minima at $\phi=\pm 90°$ so it cannot be the source of a restoring force that would prevent the dipoles from becoming ''stuck.'' However, this can again be remedied by allowing pretilt, we can then write an approximate form of the anisotropic surface energy as

$$W_S(\phi) = -2\gamma_N \sin^2\left(\frac{\phi}{\frac{\pi}{2}-\Delta}\frac{\pi}{2}\right), \tag{23}$$

where W_S has minima at $\phi=\pm(\pi/2-\Delta)$ and we confine ϕ to be in the range from $-\pi/2$ to $+\pi/2$.

C. Statics with surface forces included

The equilibrium dipole orientation is found by determining the minimum of the total potential energy,

$$W(\phi) = U(\phi)t_F = W_0\left(\sin^2\phi + 2\frac{V}{V_S}\sin\phi\right) + W_S(\phi). \tag{24}$$

The $W_S(\phi)$ potentials for the polar anchoring and pinned polar anchoring cases are qualitatively similar, they both have a minimum at $\phi=0$ and both increase as ϕ approaches $\pm\pi/2$. The case of nonpolar anchoring is qualitatively different because $W_S(\phi)$ has two minima instead of one. The locations of these minima depend on the pretilt angle and are near $\pm\pi/2$.

The total polar anchoring energy (sum of both surfaces) is scaled by $W_S=2\gamma_P$; for pinned polar anchoring, the energy is scaled by $W_S=2\gamma$. Equilibrium values of ϕ vs V/V_S are plotted in Fig. 10 for W_S/W_0 ratios of 0, 0.3, 1, and 2. A pretilt angle of $\alpha=5°$ ($\Delta=10°$) was assumed for the polar anchoring case. The effect of surface forces for $V/V_S \ll 1$ is small. At larger values of V/V_S (and thus larger ϕ) surface

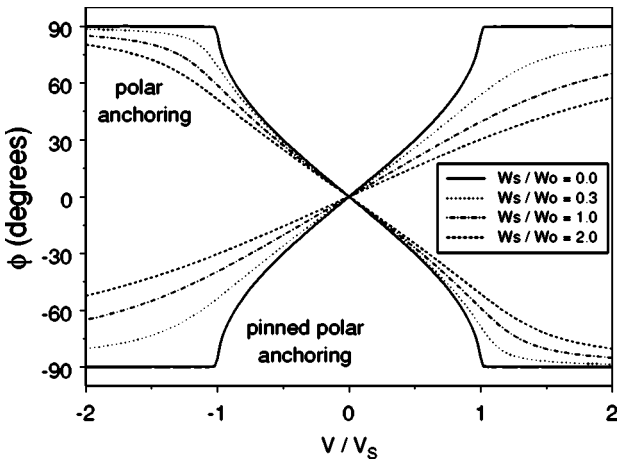

FIG. 10. Calculated equilibrium values of ϕ vs V/V_S for a range of W_S/W_0 ratios. Curves starting at the upper left are for the case of polar anchoring with 5° pretilt ($\Delta=10°$). Curves starting at the lower left are $-\phi$ for pinned polar anchoring.

forces become more important due to weakening of the $\mathbf{P}\times\mathbf{E}$ torque, causing ϕ to approach $\pm\pi/2$ only asymptotically. In calculations for the pinned polar anchoring case, W_0 and V_S are replaced by W_0' and V_S' [Eq. (15)]. Note that for pinned polar anchoring, we can rewrite Eq. (19) in the limit that $t_F \cong t_B$ and $4\xi_P/t_B \ll 1$ as

$$W_S/W_0' = \pi^2 \frac{\left(1+\frac{\varepsilon_A}{\varepsilon_F}\frac{t_F}{2t_A}\right)}{\left(1+\frac{\varepsilon_A}{\varepsilon_F}\frac{\xi_P}{t_A}\right)}\frac{\xi_P}{t_F}, \tag{25}$$

so W_S/W_0' ratios ranging from less than to greater than 1 are physically reasonable for a polarization stiffened cell, where $\xi_P/t_F \ll 1$.

The total nonpolar anchoring energy (sum of both surfaces) is scaled by $W_S=2\gamma_N$. Equilibrium values of ϕ vs W_S/W_0 are shown in Fig. 11 for $V/V_S=0,\pm 0.3,\pm 0.6$, and ± 0.9. A pretilt of zero is assumed ($\Delta=0$). For $W_S/W_0<1$

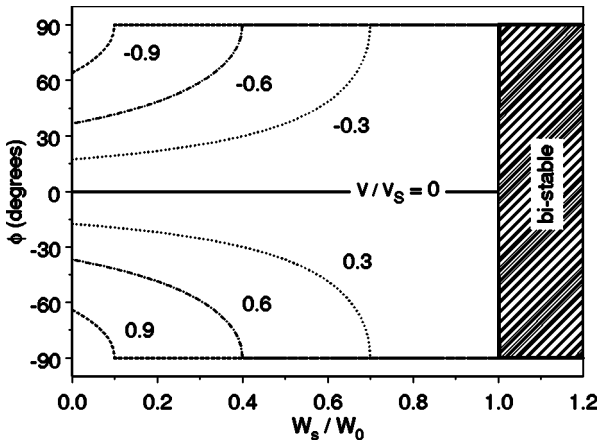

FIG. 11. Curves of equilibrium dipole orientation vs surface-to-bulk energy ratio for the case of nonpolar anchoring and zero pretilt ($\Delta=0$). Curves are shown for $V/V_S=0$, 0.3, 0.6, 0.9.

the FLC is monostable with an analog response. However, due to the nonpolar surface potential, the voltage at which the dipole rotates fully to $\pm\pi/2$ is less than V_S and depends on W_S/W_0. For $W_S/W_0>1$, the FLC becomes bistable with equilibrium states of $\phi=\pm\pi/2$. Thick alignment layers and/or large polarization favor analog behavior while thin alignment layers and/or small polarization favor bistable behavior.

Copič *et al.* [15] have performed a detailed analysis to determine conditions for monostability and bistability as functions of surface anchoring, FLC parameters, and alignment layer parameters. Unlike the simplified treatment used here, they allow the director structure to vary in response to elastic, electrostatic, and surface forces. The case of a stiffened director structure with nonpolar anchoring considered here matches a case considered in that more general treatment. That treatment also found that the boundary between monostability and bistability occurs at $W_S/W_0=1$.

Although we found that polar anchoring produces monostable analog behavior for all values of W_S, this result is nothing more than an accident due to the form chosen for $W_S(\phi)$. If, instead of $\gamma_P\sin\phi$, we had chosen some function having a sharper minimum near $\phi=-\pi/2$ and a near-constant value away from the minimum then the sum of potentials for the two surfaces could easily have two minima. Furthermore, a summed potential of this type would not need pretilt in order to be nonzero. Thus, in general, polar anchoring should also be capable of inducing bistable behavior.

D. Dynamics with surface forces included

To model switching dynamics, we need to determine the torque exerted by the surfaces on the bulk of the stiffened director structure. Torque per unit area at the surfaces is given by $T_A(\phi)=-dW(\phi)/d\phi$. Although torque is applied only at the surface, it acts uniformly throughout the cell volume because molecules are constrained to rotate together. The torque per unit volume is, therefore, the ratio of total torque divided by total volume: $T_V=AT_A/At_F=T_A/t_F$, where A is the cell area. The effect of surface torque weakens as the cell becomes thicker.

As before, we assume viscosity-limited dynamics. Including surface forces, the equation of motion is now

$$\frac{d\phi}{dt}=\frac{1}{\eta}E_F P_S\cos\phi-\frac{1}{\eta}\frac{1}{t_F}\frac{dW_S(\phi)}{d\phi}$$

$$\Rightarrow\tau_0\frac{d\phi}{dt}=-\left(\frac{V}{V_S}+\sin\phi\right)\cos\phi-\frac{1}{2W_0}\frac{dW_S(\phi)}{d\phi}. \qquad (26)$$

For constant drive voltage V, the vFLC cell will have a steady-state orientation of ϕ_V. The general expression for the time constant governing small motions of the dipole near ϕ_V is derived in Appendix B and is written in terms of the surface interaction energy $W_S(\phi)$. For pinned polar anchoring, the time constant becomes

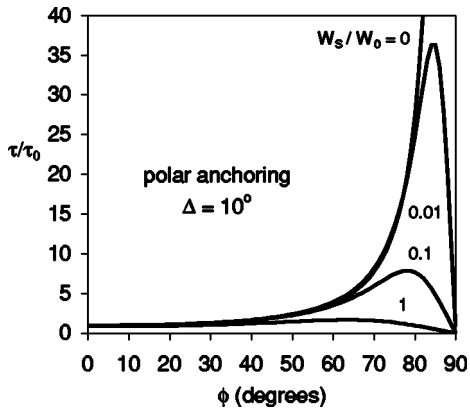

FIG. 12. Computed curves of the ϕ-dependent time constant at various values of W_S/W_0 for polar anchoring. Curves for pinned polar anchoring are similar.

$$\tau(\phi_V)=\frac{\tau_0}{\cos^2\phi_V+\dfrac{W_S}{W_0}\dfrac{2}{\pi^2}(1+\phi_V\tan\phi_V)}. \qquad (27)$$

For polar anchoring it becomes

$$\tau(\phi_V)=\frac{\tau_0}{\cos^2\phi_V+\dfrac{W_S}{W_0}\dfrac{\sin\Delta}{\cos\phi_V}}. \qquad (28)$$

The expressions for τ contain the $\cos^2\phi_V$ term responsible for divergence in the initial electrostatic model as ϕ_V approaches $\pm 90°$. Now, however, the denominators contain an additional term due to surface forces, which prevents divergence to infinity. Curves of $\tau(\phi_V)$ are shown in Fig. 12. Although τ/τ_0 can still become quite large as ϕ_V increases, it no longer grows to infinity. Large values of W_S/W_0, if physically realizable, can be exploited to prevent large, undesirable increases in τ/τ_0 which would otherwise occur.

V. THE OPTICAL MODEL

The idealized electrostatically stiffened vFLC is a uniaxial dielectric at optical frequencies, with the c axis of the optical index ellipsoid being parallel to the vFLC director. The vFLC cell acts as a wave plate for normally incident light. The projection of the index ellipsoid's c axis onto the plane of the cell determines the waveplate's optic axis orientation Θ relative to the z axis. The retardation Γ of the wave plate is a function of the index ellipsoid's ordinary and extraordinary indices of refraction n_o and n_e, and of the angle ψ which denotes the degree to which the index ellipsoid's c axis tilts out of the plane of the cell [16]:

$$\Gamma(\psi)=\frac{2\pi[n_e(\psi)-n_0]L}{\lambda}, \qquad (29)$$

$$\frac{1}{n_e^2(\psi)}=\frac{\sin^2\psi}{n_0^2}+\frac{\cos^2\psi}{n_e^2}.$$

The angles Θ and ψ are related to the dipole orientation and FLC tilt angle θ through the following relations:

$$\tan\Theta = \mp \tan\theta \sin\phi, \quad \sin^2\psi = \cos^2\phi \sin^2\theta. \tag{30}$$

The $(-)$ sign applies if the c director is clockwise from **P** as illustrated in Fig. 1, the $(+)$ sign applies if it's counterclockwise.

The standard configuration for viewing V-shaped switching is to place the vFLC cell between crossed polarizers such that the cell's z axis is parallel to the polarization state of incident light. The intensity of light transmitted by this assembly is

$$I = I_0 \sin^2[\Gamma(\psi)/2]\sin^2(2\Theta). \tag{31}$$

VI. NUMERICAL SIMULATIONS VERSUS TEST CELL

In order to compare the models to a test cell, we need to know the FLC's values of P_S, η, and ε_F, and we need to know the cell's values for t_A, ε_A, and t_F. The test cell's alignment layer was nylon-6 with $t_A = 19 \pm 2$ nm (profilometer measurement) and $\varepsilon_A \cong 5\varepsilon_0$ at 65 °C [17]. The cell gap was set to $t_F = 3.4$ μm using commercially available spacer balls.

The high-P_S FLC was MX10142 formulated at Displaytech. This deVries FLC is a 1:1 mixture of MDW1228 and MDW1248 (referred to as materials $C4$ and $C6$ in Ref. [18]). The cell was temperature stabilized in the C^* phase at 65 °C. P_S was determined by driving the cell with a ± 10 V-square wave and then integrating the cell's polarization reversal current during one FLC switching event. The polarization was computed using $P_S = Q/2A$, where Q is the integrated current and A is the cell area. Viscosity was determined by measuring the peak value of polarization reversal current I_{max} that occurs during switching [19]: $\eta = P_S^2 V / i_{max} t_F$ (for $t_A \ll t_F$) where $i_{max} = I_{max}/A$ and $V = 10$ V. Values determined for MX10142 at 65 °C were $P_S = 110$ nC/cm^2 and $\eta = 1.6$ P.

Values for the FLC's tilt angle θ and indices of refraction n_o and n_e are needed for the optical simulation. The measured value of θ is 30°. No measurement of n_o is available at $\lambda = 1.55$ μm (the wavelength used for this test). MX10142 is expected to have optical properties typical of many FLCs, so we assume $n_o = 1.5$. The cell's maximum retardation (at $\phi = \pm \pi/2$) was $\Gamma \cong 80°$, implying $n_e \cong 1.6$.

Assuming the FLC to have a typical elastic constant of $B \cong 10^{-11}$ N and estimating $\varepsilon_F = 5\varepsilon_0$, we compute $\xi_P = 19$ nm. The ratio $L/\xi_P \sim 180$ suggests that polarization stiffening should dominate in this cell allowing us to obtain analog vFLC behavior. The bulk electrostatic energy W_0 is calculated to be 0.5 erg/cm^2, which is not high enough to be certain of overwhelming surface interactions that may be as large as 1 erg/cm^2. In the case of pinned surfaces, the elastic energy γ [Eq. (17)] was calculated to be 1.3 erg/cm^2, again indicating that surface forces are probably important in this cell.

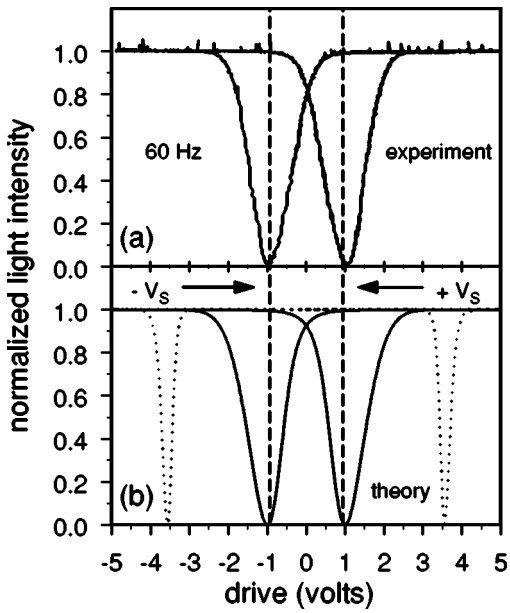

FIG. 13. (a) Measured cell response. (b) The solid line is the best-fit numerical simulation for polar anchoring (5° pretilt, $W_S = 0.3$ erg/cm^2). The dotted line is for a near zero W_S of 2×10^{-7} erg/cm^2.

The vFLC time constant τ_0 was computed by Eq. (3) to be 530 μs. The cell's actual τ_0 was checked by driving the cell with a ± 20-mV square wave and observing the settling time of the optical response $I(t) = I(0) + \Delta I(1 - e^{-t/\tau})$, this was found to be about 500 μs. Given the imperfections of the test cell (discussed below) and the simplicity of the model this level of agreement is quite good. The computed value of V_S for this cell is 0.94 V. Only the ratio of surface energy to bulk electrostatic energy remains undetermined, we have no independent measurement or calculation of W_S.

The cell was driven by a 60-Hz triangle wave having an amplitude of 5 V. The cell was placed between crossed polarizers and the transmitted light intensity (from a laser diode operating at $\lambda = 1.55$ μm) was measured as a function of V. Both the polar anchoring and pinned polar anchoring models were tried in numerical simulations which used Eq. (26) to compute the time evolution of ϕ. The ratio W_S/W_0 was varied to obtain the best match between simulation and measurement.

Using the pinned polar anchoring model, the best match between numerical simulation and measurement was obtained for a W_S/W_0 ratio corresponding to $\gamma = 0.08$ erg/cm^2. This value is more than an order of magnitude smaller than the elastic energy of $\gamma = 1.3$ erg/cm^2 computed from Eq. (17), suggesting that ϕ cannot be pinned at the surface. The discrepancy between these two values for γ indicates that the director structure is probably uniform (or nearly so) all the way to the surface and that the polar anchoring model should be used instead. The polar anchoring model produced a good match for $\gamma_P = 0.15$ erg/cm^2 with a pretilt angle of $\alpha = 5°$ ($\Delta = 10°$). Any other combination of

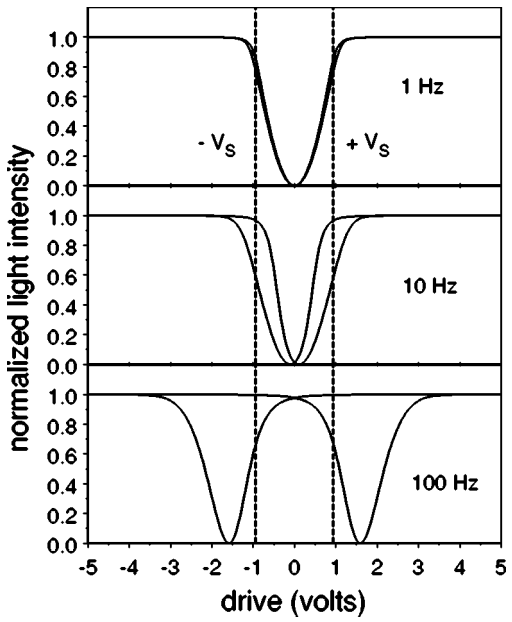

FIG. 14. Numerical simulations at three drive frequencies (triangle wave form, polar anchoring).

γ_P and Δ satisfying $\gamma_P \sin\Delta = 0.026$ is equivalent (no measurement of Δ is available). Figure 13 shows both the measured cell response and the polar anchoring numerical simulation. Their agreement is surprisingly good considering the simplicity of the model. A numerical simulation with $\gamma_P = 10^{-7}$ erg/cm^2 and 5° pretilt is shown for comparison, this is nearly equivalent to the pure electrostatic model which neglects surface interactions. Numerical simulations for smaller values of γ_P (e.g., 0) converge to steady-state behavior very slowly making these cases inconvenient to use for illustration.

Figure 14 shows numerical simulations at three-drive frequencies. At the low frequency of 1 Hz, the FLC dipole accurately follows the applied voltage, thus showing the characteristic "V" of V-shaped switching. At 10 Hz, the slow time constant occurring at large modulation amplitude is causing the vFLCs response to lag the drive wave form, causing the "V" to become distorted. At 100 Hz, the large amplitude time constant has caused the vFLC to lag so much that the "V" has become a "W."

Although the FLC cell studied here shows a good approximation to V-shaped switching, it suffers from some nonidealities. Alignment uniformity is poor due to the general difficulty of achieving good results with *I-A-C** materials lacking a nematic phase. Current flowing through the cell shows evidence of an ionic charge contribution that must have some effect on the cell's operation. Some cells exhibited more complex thresholdlike behaviors even though their construction was similar. These observations indicate that more complex mechanisms are at work in the cell than are accounted for in the model. Another concern is that x-ray data shows sufficient shrinkage of the smectic layer spacing upon cooling to cause the bookshelf layers to become deformed, although zigzags (indicating chevrons) have not been observed. Nevertheless, the degree to which the model and actual cell behavior match suggest that the model captures much of the essential physics at work in the cell.

VII. DISCUSSION

The electrostatic model of high-P_S smectic-C^* FLCs applies to the extreme case in which surface forces can be neglected. The analysis and tests reported here highlight the importance of taking surface forces into consideration in cells of practical interest, i.e., in FLC cells where P_S is large enough to fully (or near fully) stiffen the director structure yet not large enough to totally overwhelm surface forces. The analysis also explains amplitude-dependent vFLC switching speeds and how this relates to the generally faster switching of binary FLCs.

Among uncertainties of the model are surface interaction strengths and the form of anchoring energy functions. Although anchoring energies of nematic liquid crystals have been extensively studied and measured, relatively little information is available for ferroelectric liquid crystals. A better quantitative and qualitative understanding of FLC surface anchoring energies is needed both to interpret vFLC experiments and to engineer better performing vFLC cells. Important quantities such as the FLC's elastic constant B are also not accurately known.

Because the steady-state dipole orientation will be some function of the voltage V_F across the FLC layer, it may seem counterintuitive that the cell's response could be altered simply by varying the alignment layer thickness. To better understand this we can look at a simple equivalent circuit model of the FLC cell. Suppose that that the director structure is fully stiffened (or nearly so) and that the dipole orientation is governed by $\phi = f(E_F P_S)$. Here $E_F = V_F/t_F$, and function f represents the effect of elastic forces within the FLC layer (including surface forces). The FLC responds to the electrically applied torque so we have used $f(E_F P_S)$ instead of $f(V_F)$. When voltage V is applied to the cell the voltage across the FLC layer will be

$$V_F = \frac{c_A}{c_F + c_A} V + \frac{P_S \sin\phi}{c_F + c_A}, \tag{32}$$

where c_F and c_A are the capacitances per unit area of the FLC and of the alignment layers. Using $V_F = t_F f^{-1}(\phi)/P_S$ and rearranging terms we find

$$\frac{V}{V_S} = -\sin\phi + \frac{\varepsilon_F}{P_S^2}\left(1 + \frac{c_A}{c_F}\right) f^{-1}(\phi). \tag{33}$$

We see that thicker alignment layers (smaller c_A reduce the influence of $f^{-1}(\phi)$, and that its influence vanishes altogether as P_S increases. In this limit the expression reduces to $V/V_S = -\sin\phi$, in agreement with the simple electrostatic

model. Even if ϕ has a more complex dependence on V_F (e.g., hysteresis, history dependence, or bistability) the influence of FLC elastic forces are still suppressed in the limit of high P_S and thick alignment layers. Note that with a thin alignment layer the voltage V_F is nearly equal to V, and the cell may be said to be voltage controlled. With a thick alignment layer, however, the dominant effect of a change in applied voltage dV is to change the amount of charge on the FLC layer: $dq = c_A dV$. Thus the cell transitions from being voltage controlled to being charge controlled as the alignment layer thickness increases. This transition is accompanied by the growing dominance of the electrostatic potential energy W_0 over the elastic energy $W_S(\phi)$ [Eq. (24)].

Blinov *et al.* [5] have recently carried out experiments, analysis, and detailed numerical calculations of thresholdless switching in Sm-C^* FLCs, in which they do not assume polarization stiffening. They include a simplified treatment of ionic effects, which are accounted for by a uniform conductivity throughout the FLC, and they focus especially on dynamics at combinations of drive frequency and ionic conductivity where ions are important. This offers an interesting complement to a previous treatment, in which more realistic ion dynamics are included (e.g., spatially varying, time-dependent densities of positive and negative ions) but the FLC is assumed to be polarization stiffened [4]. The results of Blinov *et al.* seem consistent with results from the simpler model presented here within their range of mutual applicability, i.e., low ionic conductivity and P_S not too small. These results also highlight that it is not fundamentally necessary to have large P_S in order to obtain analog switching, it's only necessary that the cell's response to an electric field be elastic and that there cannot be multiple energy minima which would give rise to hysteresis. The analysis presented here shows that large-P_S and thick alignment layers help to create this situation by overwhelming competing mechanisms such as multiple-minima surface anchoring potentials.

It is useful to note that adding an external series capacitor is equivalent to increasing the alignment layer thickness. Key parameters can be conveniently restated in terms of the capacitances per unit area of the FLC layer c_F, and of the total external capacitance c_{Ex}, which includes the alignment layer plus any capacitance placed in series with the cell:

$$V_S = \frac{P_S}{c_{Ex}}, \qquad \tau_0 = \frac{\eta \varepsilon_F}{P_S^2}\left(1 + \frac{c_{Ex}}{c_F}\right), \qquad W_0 = \frac{1}{2}\frac{P_S^2}{c_{Ex} + c_F}. \tag{34}$$

An important topic not discussed here is the influence of ions on the vFLC polarization stiffening mechanism. Ions can be expected to weaken the stiffening mechanism and thus increase ξ_P. No calculations are available to quantitatively assess the severity of this effect, although it seems reasonable that it would be important only at low drive frequencies (ions would be too slow to follow the changing electric field at high frequencies). The ratio of Debye screening length to ξ_P might be at least a crude measure of how important ions are. That ratio is estimated to be around 10 for the cell studied here, suggesting that ions might have had only a small effect. However, a better analysis is needed.

ACKNOWLEDGMENTS

This work was funded by the DARPA Liquid Crystal Agile Beam Steering program under Contract No. DAAH01-97-C-0139 with the Rockwell Scientific Company. The author thanks Noel Clark, Mark Handschy, Michael Meadows, and Michael Wand for helpful discussions. Figure 1 is based on an illustration provided by Noel Clark. The FLC cells were built by Chris Walker who also measured alignment layer thicknesses. The FLC was supplied by Michael Wand.

APPENDIX A: DIELECTRIC ANISOTROPY

With the inclusion of dielectric anisotropy the torque equation [Eq. (3)] becomes [19]

$$\eta \frac{d\phi}{dt} = E_F P_S \cos\phi (1 - \alpha \sin\phi), \tag{A1}$$

$$\alpha \equiv \frac{\Delta\varepsilon E_F}{P_S}\sin^2\theta.$$

This is the same as Eq. (3) except for the term proportional to $\Delta\varepsilon$. Next substitute Eq. (2) for E_F into the expression for α:

$$\alpha = -\frac{\Delta\varepsilon}{\varepsilon_F(\phi)}\frac{V/V_S + \sin\phi}{1 + \dfrac{\varepsilon_A}{\varepsilon_F(\phi)}\dfrac{t_F}{2t_A}}\sin^2\theta. \tag{A2}$$

In general, $\theta < 45°$ ($\sin^2\theta < 1/2$), V/V_S is on the order of 1 or less, $\Delta\varepsilon/\varepsilon_F < 1$, $\varepsilon_A/\varepsilon_F < 1$, and $t_F/2t_A > 1$, therefore $\alpha < 1$. In most cases of interest, the alignment layers are much thinner than the FLC layer ($t_F/2t_A > 10$) so we have $\alpha \ll 1$. Therefore, the term proportional to $\Delta\varepsilon$ in the torque equation can be omitted.

APPENDIX B: SMALL SIGNAL RESPONSE

The general form of the dynamical equation is

$$\tau_0 \frac{d\phi}{dt} = f(\mathcal{V}, \phi), \tag{B1}$$

where from Eq. (26), we have

$$f(\mathcal{V},\phi)=-\left(\frac{\mathcal{V}}{V_S}+\sin\phi\right)\cos\phi-\frac{1}{2W_0}\frac{dW_S(\phi)}{d\phi}. \quad \text{(B2)}$$

The first-order series expansion of f about the point $(\mathcal{V},\phi)=(V,\phi_V)$ is

$$f(\mathcal{V},\phi)\cong f(V,\phi_V)+\left.\frac{\partial f}{\partial\mathcal{V}}\right|_{\substack{\mathcal{V}=V\\ \phi=\phi_V}} d\mathcal{V}+\left.\frac{\partial f}{\partial\phi}\right|_{\substack{\mathcal{V}=V\\ \phi=\phi_V}} d\phi. \quad \text{(B3)}$$

We choose (V,ϕ_V) to be a steady-state solution of Eq. (B1), where $d\phi/dt=0$ [thus $f(V,\phi_V)=0$], since we are interested in small perturbations about equilibrium.

After evaluating the derivatives, we obtain

$$\frac{d\tilde{\phi}}{dt}=-\frac{\cos\phi_V}{\tau_0}\frac{v(t)}{V_S}-\frac{1}{\tau(\phi_V)}\tilde{\phi}\tau(\phi_V)$$

$$=\frac{\tau_0}{\cos^2\phi_V+\frac{1}{2W_0}\left(\tan\phi_V\left.\frac{dW_S(\phi)}{d\phi}\right|_{\phi_V}+\left.\frac{d^2W_S(\phi)}{d\phi^2}\right|_{\phi_V}\right)}. \quad \text{(B4)}$$

We have made the substitutions $d\mathcal{V}=v(t)$, where $v(t)$ is a small time-dependent voltage, and $d\phi=\tilde{\phi}$ is a small deviation around the equilibrium position ϕ_V. The fact that $f(V,\phi_V)$ is zero was used to simplify the result of evaluating $\partial f/\partial\mathcal{V}$, an expression containing both V and ϕ_V was simplified to contain only ϕ_V.

[1] S. Inui, N. Iimura, T. Suzuki, H. Iwane, K. Miyachi, Y. Takanishi, and A. Fukuda, J. Mater. Chem. **6**, 671 (1996).

[2] P. Rudquist, J.P.F. Lagerwall, M. Buivydas, F. Gouda, S.T. Lagerwall, N.A. Clark, J.E. Maclennan, R. Shao, D.A. Coleman, S. Bardon, T. Bellini, D.R. Link, G. Natale, M.A. Glaser, D.M. Walba, M.D. Wand, and X.-H. Chen, J. Mater. Chem. **9**, 1257 (1999).

[3] N.A. Clark, D. Coleman, and J.E. Maclennan, Liq. Cryst. **27**, 985 (2000).

[4] M. Čopič, J.E. Maclennan, and N.A. Clark, Phys. Rev. E **63**, 031703 (2001).

[5] L.M. Blinov, E.P. Pozhidaev, F.V. Podgornov, S.A. Pikin, S.P. Palto, A. Sinha, A. Yasuda, S. Hashimoto, and W. Haase, Phys. Rev. E **66**, 021701 (2002).

[6] Sven T. Lagerwall, *Ferroelectric and Antiferroelectric Liquid Crystals* (Wiley-VCH/Verlag, Weinheim, 1999).

[7] Z. Zhuang, J.E. Maclennan, and N.A. Clark, Proc. SPIE **1080**, 110 (1989).

[8] Jacob N. Israelchvili, *Intermolecular and Surface Forces*, 2nd ed. (Academic Press, New York, 1992).

[9] Jacques Cognard, Mol. Cryst. Liq. Cryst. Suppl. Ser. **A5**, 1 (1982).

[10] A. A. Sonin, *The Surface Physics of Liquid Crystals* (Gordon and Breach, London, 1995).

[11] Jiuzhi Xue, Ph. D. thesis, University of Colorado, 1989 (unpublished).

[12] I. Dahl, Ferroelectrics **84,** 327 (1988).

[13] Z. Zhuang, Ph. D. thesis, University of Colorado, 1991 (unpublished).

[14] M.A. Handschy, N.A. Clark, and S.T. Lagerwall, Phys. Rev. Lett. **51**, 471 (1983).

[15] Martin Čopič, Joseph E. Maclennan, and Noel A. Clark, Phys. Rev. E **65**, 021708 (2002).

[16] Amnon Yariv and Pochi Yeh, *Optical Waves in Crystals* (Wiley, New York, 1984).

[17] *Polymer Handbook*, 3rd ed., edited by J. Brandrup, E. H. Immergut (Wiley, New York, 1989).

[18] N.A. Clark, T. Bellini, R.-F. Shao, D. Coleman, S. Bardon, D.R. Link, J.E. Maclennan, X.-H. Chen, M.D. Wand, D.M. Walba, P. Rudquist, and S.T. Lagerwall, Appl. Phys. Lett. **80(22)**, 4097 (2002).

[19] Xue Jiu-Zhi, M.A. Handschy, and N.A. Clark, Ferroelectrics **73**, 305 (1987).